PCCP

Accepted Manuscript

ROYAL SOCIETY OF CHEMISTRY

www.rsc.org/pccp

Journal Name

ARTICLE TYPE

Cite this: DOI: 10.1039/xxxxxxxxxx

Impact of Tellurium on the Structure and ^{77}Se NMR Spectra of Selenium-Rich Ternary Ge-Te-Se Glasses: a combined experimental and computational investigation†

Lila Bouëssel du Bourg,[a] Claire Roiland,[b], Laurent le Pollès,[a] Michaël Deschamps,[c] Catherine Boussard-Plédel,[b] Bruno Bureau,[b] Chris J. Pickard[d] and Eric Furet*[a]

Received Date
Accepted Date

DOI: 10.1039/xxxxxxxxxx

www.rsc.org/journalname

Selenium-rich Ge-Te-Se glasses have been synthesized along the $GeSe_4$-$GeTe_4$ pseudo-composition line and acquired by ^{77}Se Hahn echo magic-angle spinning NMR. The comparison with the $GeSe_4$ spectrum shows a drastic modification of the typical double-resonance lineshape even at low Te concentrations (<10%). In order to rationalize this feature and to understand the role of Te on the structure of our glasses, first-principles molecular dynamics simulations and *gauge including projector augmented wave* NMR parameters calculations have been performed. The distribution of the tellurium atoms in the selenium phase was shown to be mainly responsible of the ^{77}Se lineshape changes. Another possible factor related to the perturbation of the δ_{iso} due to Te proximity appears much more limited in the bulk, while results obtained with molecular models suggest shifts of several hundredth of ppm.

1 Introduction

Chalcogenide glasses have been widely studied over the past decades for their manifold properties.[1,2] Among those, they are known to show reversible amorphous-to-crystal transition, high linear and nonlinear refractive indices and large infrared transparency windows that covers the two atmospheric windows (3-5 μm and 8-12 μm).[3] Some of them are also exhibiting original light-induced phenomena or potentially interesting thermoelectric properties. For thermal imaging or *in situ* spectroscopy, telluride glasses are very promising since they possess the largest transmission windows in mid-IR (up to 26 μm) and give access to wavelength range which is not reachable with selenide glasses.[4–11]

However, Te-based glasses have complicated syntheses, because they are prone to devitrification processes and usually only give micro-samples. They were moreover originally rather developed for reversible glass-to-crystal transformation for optical storage applications.[12–15] In a previous work, Maurugeon *et al*[16–18] have shown that the introduction of even a few percents of Se in the binary Ge-Te system makes the corresponding glasses much easier to prepare and more stable against crystallisation, while keeping large transparency in the mid-infrared. However, their inner structure is still not well established because only a couple of studies have been carried out so far on this ternary system.[19–21] Among the available experimental spectroscopic techniques, solid-state NMR (ssNMR) measurements appear to be a suitable tool to contribute to the elucidation of their structure at the atomic scale.

In the framework of a research project devoted to this family of ternary glasses, we will present here results gathered on the selenium-rich side of the $GeSe_4$-$GeTe_4$ pseudo-composition line,[16] in order to investigate the precise role of low fraction of Te on the structure of these glasses. This will allow to take advantage of the high Se percentage, that can be much more easily acquired than the ^{125}Te or the quadrupolar ^{73}Ge isotopes.[22,23] Indeed, it has been recently demonstrated that quantitative ^{77}Se ssNMR spectra could be acquired on the $GeSe_4$ parent composi-

[a] *Institut des Sciences Chimiques de Rennes, UMR-CNRS 6226, Ecole Nationale Supérieure de Chimie de Rennes, 35708 Rennes, France. Fax: +33 2 2323 8199; Tel: +33 2 2323 8106; E-mail: eric.furet@ensc-rennes.fr*

[b] *Institut des Sciences Chimiques de Rennes, UMR-CNRS 6226, Université de Rennes 1, 35042 Rennes cedex, France.*

[c] *CNRS, CEMHTI UPR 3079, Univ. Orléans, 45071 Orléans, France*

[d] *Department of Physics and Astronomy, University College London, Gower Street, London WC1E 6BT, UK*

† Electronic Supplementary Information (ESI) available: (Figure S1) ^{77}Se NMR spectrum of $Ge_{20}Se_{20}Te_{60}$, (Figure S2) individual coordination mode histograms for the six Ge-Te-Se models, (Figure S3) Se-Se, Se-Se and Se-Te pair correlation functions for the six Ge-Te-Se trajectories, (Figure S4) Visualisation of two structures of our glass models together with tetrahedra for the Ge coordination spheres, (Figure S5) Averaged Se-Te pair correlation functions and integrations for the two sets of Ge-Te-Se glasses, (Table S1) numerical values for the six Ge-Te-Se 300 K trajectories. See DOI: 10.1039/b000000x/

tion that proved to be useful for the glass structure understanding.[24,25] This will also offer the opportunity to investigate the performances of the *Gauge Including Projector Augmented Wave* (GIPAW)[26] formalism to reproduce experimental data when heavy atoms such as Te are present in the material.

2 Experimental and Theoretical Methods

2.1 Glass Synthesis

Glasses of general formula $Ge_{20}Se_{80-x}Te_x$, were synthesized in silica tube in order to avoid contamination. During the chemical purification step, Te (6N), Ge (5N) and Se (6N) were weighed in the adequate proportion. The melted mixtures were distilled through a filter to a reaction silica tube so as to trap impurities. The reaction tube was then sealed under vacuum and homogenized at 750 °C for 10 hours. Bulk glasses were obtained after quenching in water and annealing. Their glassy state was confirmed by X-ray power diffraction (XRD) and differential scanning calorimetry (DSC). The final glass compositions was checked by EDS (Energy Dispersive Spectroscopy). They were in agreement with the initial stoechiometry within the error bar of the measurements that were equal to 1%. The vitreous transition temperatures were found to be respectively 165 °C (x=0), 165 °C (x=10), 170 °C (x=20), 157 °C (x=60). Note that between x=20 and x=60, there is a demixing zone, where it is not possible to form glass.

2.2 Solid-State NMR Experiments

^{77}Se (I = 1/2) Hahn echo magic-angle spinning (MAS) NMR experiments were performed on a Bruker Avance 300 spectrometer (7.1T) operating at a Larmor frequency of 57.3 MHz for ^{77}Se, using a 4.0 mm Bruker probe. To ensure a complete relaxation of the ^{77}Se magnetization and quantitative measurements, a recycling delay of 300 s (D1) was used between each of the scans. The ^{77}Se chemical shift was referenced to H_2SeO_3 saturated in water at 1288 ppm. The spinning frequency was set to 14 kHz to reduce the intensities of the spinning sidebands.

2.3 Molecular dynamics computational details

Car-Parrinello calculations[27] were carried out using the CPMD-3.17.1 code.[28–30] We employed the Perdew-Burke-Ernzerhof (PBE) exchange and correlation (XC) functionals.[31] The valence-core interactions were described by means of norm-conserving pseudo-potentials according to the Troullier-Martins scheme.[32,33] Valence electrons were represented in a plane-wave basis set with an energy cut-off of 20 Ry and the calculations were done at the Γ point of the Brillouin zone. The temperature was controlled using Nosé-Hoover thermostat chains.[34,35] An integration step of 7 u.a. (0.17 fs) and a fictitious electronic mass of 850 u.a. were employed so as to ensure a good control of the conserved quantities all along the trajectories. The *in silico* glass syntheses were performed with cubic cells of 18.3 x 18.3 x 18.3 Å^3 containing a total of 215 atoms.

The Ge-Te-Se starting configurations were derived from two independent $GeSe_4$ grain models, labelled here G_1 and G_2, built according to a procedure that was previously demonstrated to allow to restore the agreement between theoretical and experimental ^{77}Se NMR spectra.[24] After a mixing phase of the $GeSe_4$ heterogeneous models for about 50 ps, at 900 K, three different ways to substitute 10% of the Se atoms by Te were used on G_1 and G_2 snapshot configurations. These six different selenium-rich cells, denoted here R_{Se1-3} and $R_{Se1'-3'}$, were then equilibrated in the liquid state (∼800K) for up to 35 ps and subsequently gradually quenched in plateaus of ∼20 ps, separated by 200 K. The statistical averages were then collected after reaching the plateau at 300 K, over more than 20 ps.

2.4 Solid-state NMR computational details

All ^{77}Se NMR parameters were computed using the *Gauge Including Projector Augmented Wave* (GIPAW) formalism as implemented in the CASTEP package, version 7.01.[36] We used the PBE XC functionals, on-the-fly generated ultrasoft pseudopotentials and an expansion of the plane-wave basis sets up to an energy cutoff of 500 eV (36.7 Ry). The Brillouin zone was sampled using a 2 x 2 x 2 k-points grid. Those values have been previously found to give accurate ^{77}Se ssNMR results on $GeSe_4$ glass cells.[24]

The GIPAW calculations give access to the absolute shielding tensor (σ) whose diagonalisation of the symmetric part leads to the three orthogonal principal components. The eigenvalues (σ_{ii}) were transformed into the three principal chemical shift components. They were ordered according to the Haeberlen convention,[37] $|\sigma_{zz} - \sigma_{iso}| > |\sigma_{xx} - \sigma_{iso}| > |\sigma_{yy} - \sigma_{iso}|$ where $\sigma_{iso} = (\sigma_{xx} + \sigma_{yy} + \sigma_{zz})/3$. The reduced anisotropy (σ_{aniso}) and asymmetry parameters (η) were computed as $\sigma_{aniso} = \sigma_{zz} - \sigma_{iso}$ and $\eta = (\sigma_{xx} + \sigma_{yy})/\sigma_{aniso}$. The isotropic chemical shift is defined as $\delta_{iso} = \sigma_{ref} - \sigma_{iso}$, where σ_{ref} is the isotropic chemical shielding of a reference compound. Calculations on the α-selenium crystalline phase gave σ_{ref} = 1483 ppm. The spectra have been simulated with the Simpson program,[38] that allows an emulation of the experimental acquisition process and to explicitly take into account all the pertinent NMR parameters in the process. In order to generate the signal of the various kind of Se environments, *i.e.* to obtain the decomposition of the total signal, the selenium sites were grouped on the basis of their respective coordination spheres and subsequently processed together with the Simpson program. Consequently, the signals are obtained by summing the individual responses of the Se nuclei and their widths is the result of the chemical shift distributions.

3 Results and Discussion

^{77}Se ssNMR measurements have been performed on glasses for the parent composition $GeSe_4$ and for Te-containing samples, namely $Ge_{20}Se_{70}Te_{10}$, $Ge_{20}Se_{50}Te_{30}$ and $Ge_{20}Se_{20}Te_{60}$. A recycling delay of 300 s was used in the experiments, as we have recently shown that very long D1 values were mandatory in order to obtain quantitative ^{77}Se NMR data.[24] Figure 1 contains the Hahn echo spectra acquired under MAS conditions for three of our compositions. Due to the low natural abundance of the ^{77}Se isotope (7%), the signal/noise of the $Ge_{20}Se_{20}Te_{60}$ spectrum is too low to consider the acquired signal as fully quantitative and consequently it will be reported in the ESI section (Figure S1).† For the other spectra, it is immediately seen that, with respect to $GeSe_4$,

a strong modification of the line shape occurs, even for substitution fractions of Se by Te as low as 10%. Indeed, the spectrum of $Ge_{20}Se_{70}Te_{10}$ is already characterized by a sole resonance that exhibits an asymmetric shape and is centered around 500 ppm. This chemical shift value corresponds mostly to the case of Ge-Se-X (X=Ge,Se) environments in $GeSe_4$. This suggests therefore an almost complete disappearance of the selenium chains line and/or its merging with the resonances associated to Se atoms bonded to at least one Ge, despite the fact that we may have up to seven times less Te than Se. The asymmetric shape of the $Ge_{20}Se_{70}Te_{10}$ spectrum and the somewhat narrowing of the signal width on going from $Ge_{20}Se_{70}Te_{10}$ to $Ge_{20}Se_{50}Te_{30}$ may give additional credit to these findings. It should be stressed that in a previous ^{77}Se and ^{125}Te NMR investigation devoted to $Se_xTe_{(1-x)}$ glasses, Bureau *et al*[39] have achieved a deconvolution of some ^{77}Se NMR signals on the basis of three contributions. These resonances located at 850, 700 and 500 ppm were attributed to Se-Se-Se, Se-Se-Te and Te-Se-Te environments respectively. Such results suggest therefore that if sufficient Te-Se-X (X=Se,Te) units are present in our Ge-Te-Se glasses, a shift of the selenium chains line may occur, leading to the potential coalescence of all the peaks into a unique one as proposed above.

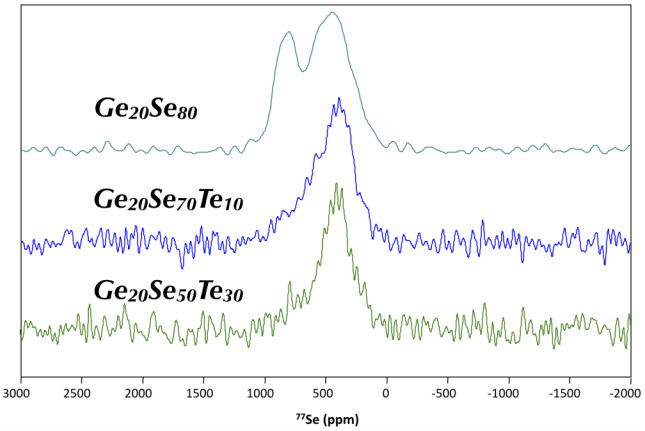

Fig. 1 ^{77}Se ssNMR spectra (from top to bottom) of $GeSe_4$ (denoted here $Ge_{20}Se_{80}$), $Ge_{20}Se_{70}Te_{10}$ and $Ge_{20}Se_{50}Te_{30}$ acquired at 300MHz (7.1 T) using a 4 mm probe and MAS rotation conditions of 14kHz.

In order to check and possibly discriminate between these assumptions, molecular dynamics have been performed to produce *in silico* samples and coupled to ^{77}Se NMR parameters calculations to obtain the theoretical spectra. Three different substitutions schemes have been used starting from two independent $GeSe_4$ trajectories in the liquid state (see computational details). Examination of the coordination spheres of the germanium atoms (Figure 2) shows that they almost exclusively obey the 8-N rule and possess four nearest neighbors disposed in the expected tetrahedral fashion (Figure 3).

Indeed, whatever the model, more than 87% of the Ge atoms are 4-fold coordinated and the angle distribution functions always exhibit a single maximum centered at 109°. Thus, our selenium-rich models, denoted here R_{Se1-3} & $R_{Se1'-3'}$, show strong similarities with their parent composition and the incorporation of

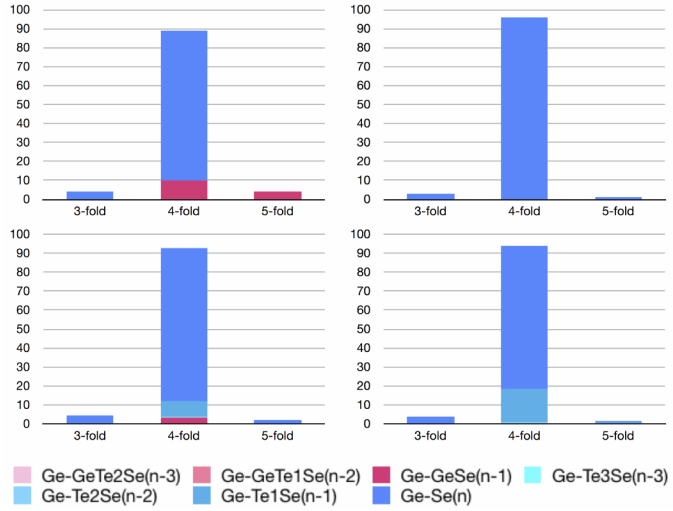

Fig. 2 Distributions of the coordinations modes for the germanium atoms at 300K, for the G_1 (top left) and G_2 (top right) binary models, and for the Te-substituted compositions (bottom). For the sake of clarity, the histogram below each $GeSe_4$ model corresponds to the average of the three Ge-Te-Se derived glasses. The individual histograms of the six Ge-Te-Se models are given in figure S2 and detailed numerical values in Table S1.†

small amounts of tellurium does not play, *per se*, a significant role on the germanium coordination spheres. Recent molecular dynamics simulations on $Ge_{20}Te_{80}$ or on $Ge_{15}Te_{85}$ have shown, however, that the fraction of GeX_4 (X=Ge, Te) units were much lower in theses cases and that a wider spectrum of Ge environments, ranging from three- to six-fold coordination modes, were observed.[40,41]

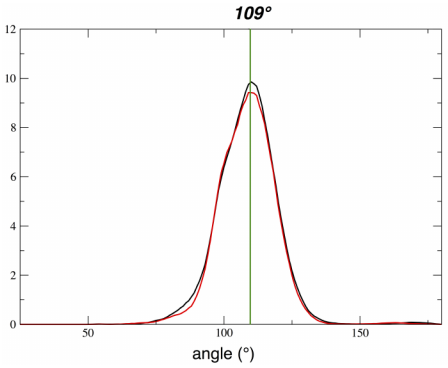

Fig. 3 Se-Ge-Se angular distribution functions calculated at 300K for the G_1 model (black line) and for our Te-substituted compositions (red line). For the sake of clarity, the six Ge-Te-Se glasses trajectories have been concatenated to obtain a single angular distribution function.

A closer inspection to the nature of the germanium coordination spheres in our Ge-Te-Se glasses shows that the number of Te bonded to Ge is truly low and corresponds almost exclusively to the case of a unique Te neighbor (Figure 2). Indeed, the computed fractions of Ge-Te bonds, that can be deduced from Table 1, range from 6.8 (R_{Se1}) to 25.6% ($R_{Se2'}$). In the randomly substituted starting configurations (see computational details), the same quantities were calculated to span values between 37.2 and 53.5%. Also, a non negligible percentage of Ge

bonded to up to three tellurium atoms could be found. Consequently, it appears from our simulations that the tellurium atoms are expelled from the germanium coordination spheres during the liquid-phase stage of the dynamics. These results thus suggest a better affinity of selenium towards germanium with respect to tellurium, that may be related to the Ge-Te and Ge-Se bond formations.[21,42] Indeed, experimentally deduced and calculated bond dissociation energies for Ge-Te molecule are found to be lower by ~20 kcal.mol^{-1} with respect to the same quantity for Ge-Se.[43] It must be noted that additional insights into the bonding nature of these glasses may possibly be achieved through the recently introduced *bond-weighted distribution function*, once this bonding indicator has been implemented in our simulation codes.[44]

Table 1 Nature of the Ge coordination spheres (%) for our six selenium-rich Ge-Te-Se glasses, calculated at 300 K, on their respective plateau. *n* denotes the coordination number ranging between 3 to 6. Detailed individual numerical values are available in Table S1.†

		G_1			G_2	
Ge coordination	R_{Se1}	R_{Se2}	R_{Se3}	$R_{Se1'}$	$R_{Se2'}$	$R_{Se3'}$
Ge-GeSe$_{n-1}$	0.0	0.0	9.2	1.5	0.0	0.0
Ge-TeSe$_{n-1}$	6.8	9.3	9.3	14.0	21.0	16.3
Ge-Te$_2$Se$_{n-2}$	0.0	2.3	0.0	0.0	2.3	0.0
Ge-Se$_n$	92.7	88.0	81.4	83.8	75.7	83.9

As for the distribution of the Te atoms in the selenium phase, our simulations do not show any significant evidence of the beginning of a segregation between the two chalcogens (Figure 4). It is indeed well known that there is a demixing zone around the middle of the GeSe$_4$-GeTe$_4$ pseudocomposition line,[16] while in our case the Te atoms appear to be rather evenly spread all over the Se phase. On the quantitative side, a selected set of averaged pair correlation functions (g(X-Y)) for our R_{Se} models and the ones corresponding to their respective GeSe$_4$ counterparts are reported in Figure 5. For the sake of completeness, the plots of the individual functions for the various R_{Se} samples are reported in the ESI section (Figure S3).†

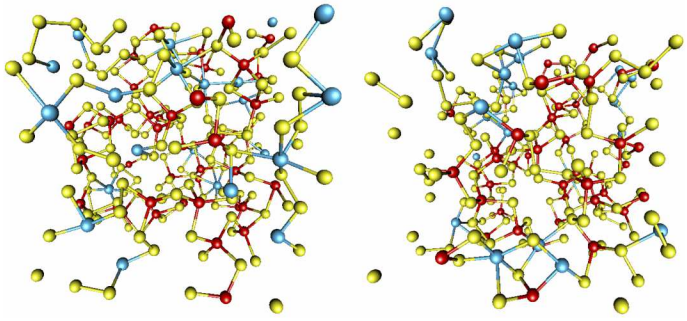

Fig. 4 Visualisation of two structures at 300K of our selenium-rich glasses derived from the G_1 (left) and G_2 (right) models. The germanium atoms are in red, the selenium atoms in yellow and the tellurium atoms in light blue (Colors online). Snapshots with tetrahedra for the Ge coordination spheres are given in figure S4.†

As expected from the results presented above concerning Ge coordination spheres, the g(Ge-Se) functions can be hardly distinguished. On the other hand, the height of the first maximum

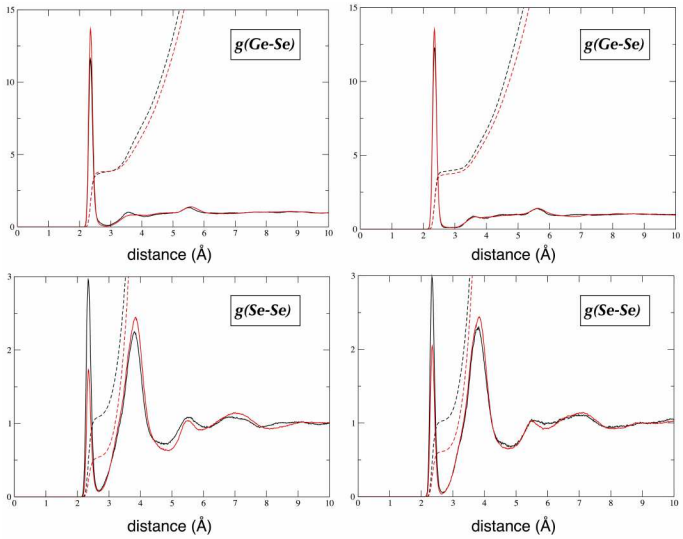

Fig. 5 Averaged Ge-Se (top row) and Se-Se (bottom row) radial distribution functions (solid line) and their integrations (dashed line) for our Ge-Te-Se glasses (red) derived from the G_1 model (left column) or from the G_2 model (right column). The RDFs for the G_1 and G_2 parent composition are also given (black) (Colors online).

of g(Se-Se) is higher in GeSe$_4$ with respect to our Te-substituted glasses. For an integration radius up to R=2.7 Å, corresponding to the position of the first minimum, values of 1.0-1.1 and 0.5-0.6 were computed for our GeSe$_4$ and Ge-Te-Se cells respectively. Concerning the fraction of Se involved in homopolar bonds (N_{Se-Se}), we calculated values that are close to 70% for the two parent glasses and are consistent with previously published results using different models or/and functionals.[45,46] For our Ge-Te-Se models, this quantity drops to significantly lower values ranging between 45.0 and 51.4%, with an average value of 47.0%. All of these numerical results, together with the shape of the g(Se-Te) functions (Figure S5)† and their integrations up to R = 3.2 Å, that is found to be always within 0.4-0.5, suggest a general tendency of the tellurium atoms to be rather evenly dispersed in the selenium chains. This phenomenon consequently leads to their splitting into shorter subchains, which should therefore have a significant impact on the Se-Se-Se NMR line.

Figure 6 presents spectra simulated with the Simpson program, using ^{77}Se NMR parameters calculated on optimized configurations taken from the 300K plateaus of our Ge-Te-Se models. A separation has been made in order to clearly identify the contributions to the various kinds of selenium environments, namely Se-Se-Se, Ge-Se-Se, Ge-Se-Ge and X-Se-Y (X=Te, Y=Ge/Se/Te). For the sake of comparison, the spectra of the corresponding GeSe$_4$ parent glasses are also given together with the main contributions, *i.e.* Se-Se-Se and Ge-Se-Se. It is immediately seen that our theoretical spectra are in very good agreement with the experimental ones (Figure 1). We obtain in all cases, a unique maximum that is centered on the so-called GeSe$_2$ phase peak of the GeSe$_4$ parent glasses. As suggested above, this is mainly related to the strong reduction of the Se-Se-Se resonance (Figure 6) that almost disappears in the R_{Se} samples, but may still survive so as to contribute to the asymmetric shape of the total signal. Indeed, in

the two parent structures, the numbers of Se-Se-Se environments are found fortuitously identical and equal to 61, corresponding therefore to nearly 35.5% of the selenium atoms. In the Ge-Te-Se glasses derived from G_2, this same quantity ranges from 10 (6.6 %) to 21 (14.8 %), with a mean value of 16.0 (10.6 %). For the case of those obtained from G_1, we have values between 8 (5.3 %) and 16 (10.6 %) corresponding to an average value of 11.7 (7.8 %). Therefore, whatever the Ge-Te-Se model considered, a significant drop of the Se-Se-Se environment is calculated.

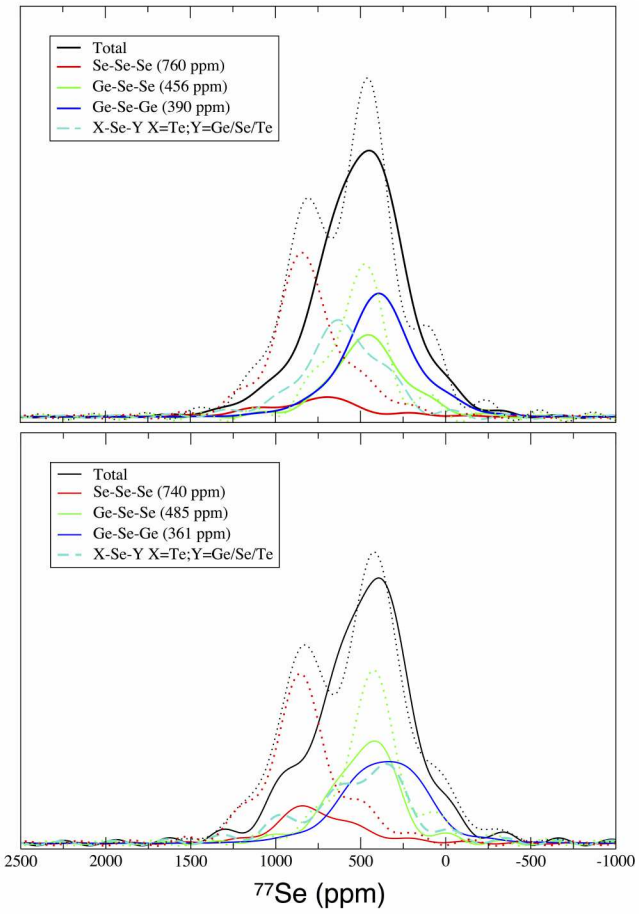

Fig. 6 ^{77}Se NMR spectra of optimized configurations taken from the 300K plateaus of one Ge-Te-Se glass derived from G_1 (bottom) and one derived from G_2 (top). Contributions of various environments are given together with their mean δ_{iso} values. The solid lines are associated to the Ge-Te-Se glasses, while the dotted lines correspond to the total spectra and the main contributions from the G_1 and G_2 binary models.

Concerning the impact of Te on the ^{77}Se δ_{iso} values, Figure 7 shows side-by-side snapshots of the G_1 parent composition and one of their Ge-Te-Se derived models. Qualitatively speaking, the perturbation induced by the presence of the tellurium atoms can be readily detected, due to the low number of Se atoms bearing large radii in the Ge-Te-Se glass. Interestingly, on the right-hand side of the Ge-Te-Se configuration, a chain of chalcogenides can be seen, illustrating the intimate mixing of Te and Se.

An analysis of the impact of Te on the ^{77}Se NMR parameters is given in Table 2. It can be seen that on average, Se-Se-Te and Te-Se-Te are characterized by lower chemical shifts values,

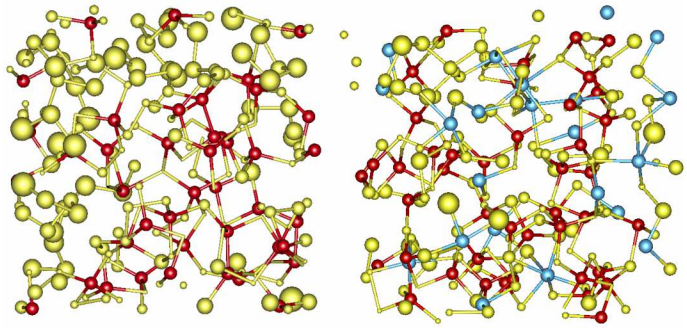

Fig. 7 Visualisation of two glass structures, one from the G_1 model (left) and another from a selenium-rich composition (right). The radius of the selenium atoms is proportional to their computed δ_{iso} values. The germanium atoms are in red, the selenium atoms in yellow and the tellurium atoms in light blue (Colors online).

with respect to the one associated to the Se chains that resonate around 770 ppm, on average. It should be pointed out that while the number of selenium atoms bonded to two tellurium atoms is really low (average value of 4.2 sites *per* Ge-Te-Se cell model) the tendency is kept, *i.e.* the more Te atoms are found around a Se atom, the lower the computed δ_{iso} value. This feature may be qualitatively rationalized on the basis of an increased shielding of the ^{77}Se nuclei, correlated to the presence of the large tellurium electron cloud(s), that should be attracted by the slightly more electronegative Se atoms. Concerning the Ge-Se-X (X=Te,Se) environments, the results are less obvious. Indeed the models derived from G_2 show on average, an opposite evolution with respect to the three other Ge-Te-Se glass cells, *i.e.* an increase instead of a lowering of the δ_{iso} values related to the presence of Te. A possible statistical *bias* due to too few Ge-Se-Te environments is not relevant here, because the total number of sites equals 194 and 140 (32.3 and 23.3 on average) for Ge-Se-Se and Ge-Se-Te respectively which corresponds to meaningful quantities.

Table 2 Averaged isotropic chemical shifts (ppm), corresponding standard deviations (ppm) and total number of sites for each set of three selenium-rich glasses derived from the two $GeSe_4$ parent compositions.

	R_{Se1-3}			$R_{Se1'-3'}$		
X-Se-Y env^f	δ_{iso}	σ	n	δ_{iso}	σ	n
Se-Se-Se	739.0	146.9	35	787.7	164.0	48
Se-Se-Te	682.4	229.1	51	678.1	200.6	51
Te-Se-Te	589.6	242.3	15	446.8	337.7	10
Ge-Se-Ge	386.2	182.6	141	396.7	171.1	135
Ge-Se-Se	470.9	150.5	102	483.9	136.8	92
Ge-Se-Te	439.2	209.3	77	546.6	203.1	63

In order to confirm the above observed trends and get rid of the perturbations due to surrounding structures in the bulk, we have built in a way similar to a previous As_xSe_{1-x} glasses investigation,[47] a set of hydrogen-terminated molecular models containing Se, Te and/or Ge (Figure 8). From model **1**, we see that the calculated ^{77}Se δ_{iso} values are quite consistent with the 800 ppm found in cristalline Se, while being only slightly overestimated. The impact of the presence of tellurium can be readily seen in **2**, **3** and **4**. Numerically speaking, the presence of one Te in the Se coordination sphere induces a lowering of the ^{77}Se

isotropic chemical shifts by about 200 ppm. Model **4** shows that the second-neighbor (H-Se-**Se**-Se-Te-H) of the tellurium atom is almost unaffected, with a ^{77}Se δ_{iso} value that remains close to the 900 ppm found in **1**. This observation suggests that the perturbation induced by a Te atom is not of the long-range kind, but limited to its immediate surroundings (no delocalization). If there is two Te bonded to Se (**3**), the ^{77}Se isotropic chemical shift value further decreases by 250 ppm leading to a global reduction of almost 500 ppm with respect to **1**. This result therefore confirms our earlier observation made on Te-Se-Te environment in the bulk, but for which the number of sites was very limited, casting some doubts on the additive impact of having several Te bound to Se. To conclude on these molecular models, **5** and **6** demonstrate the very strong perturbation induced by germanium atoms on their first-neighbor Se atoms, with δ_{iso} that drops below 300 ppm. This is in complete agreement with the position of the Ge-Se-Ge and Ge-Se-Se resonances in our Ge-Te-Se models (Figure 6 - Table 2) and the position of the $GeSe_2$ phase line in $GeSe_4$ (Figure 1). Finally, like Te, the short range behavior of the Ge perturbation can be seen in **6**, with a selenium second-neighbor that recovers the expected 800 ppm ^{77}Se δ_{iso} value, typical of a Se-Se-Se unit.

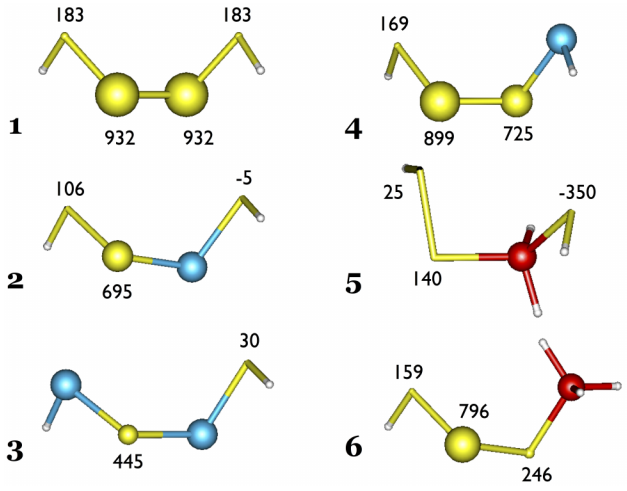

Fig. 8 Optimized structures of molecular models with the radius of the Se atoms proportional to their respective computed δ_{iso} values. The isotropic chemical shifts of only the ^{77}Se are given. Hydrogen, selenium, tellurium and germanium atoms are white, yellow, light blue and red respectively (Colors online).

4 Conclusions

^{77}Se solid-state NMR measurements and Car-Parrinello molecular dynamics coupled to GIPAW calculations have been performed to investigate the structural and NMR spectroscopic properties of selenium-rich glasses, along the $GeSe_4$-$GeTe_4$ pseudo-composition line. From the solid-state NMR experimental data, it appears that a drastic change in the spectrum lineshape occurs, even for Te fractions as low as 10%, like in the $Ge_{20}Se_{70}Te_{10}$ composition. The disappearance of the selenium phase resonance may consequently be attributed to a reduction of the Se chains, despite the very low concentration of Te, and/or to the impact of the tellurium atom on the chemical shifts.

The analysis of the molecular dynamics structures has shown that the tellurium avoids to bind to germanium atoms. The expelled tellurium appears to be dispersed in the Se chains, thus leading to a significant drop of the number of Se-Se-Se environments. The simulation of the ^{77}Se NMR spectra demonstrates that this factor is mainly responsible of the experimentally detected lineshape changes. The second factor associated to shielding perturbations, due to Te short-range influence, has also an impact. This seems however more limited, at least in the glass material, probably due to a competition with other factors impacting the isotropic chemical shifts in the bulk.

5 Acknowledgements

This work was granted access to the HPC resources of IDRIS, CINES and TGCC under the allocation 2015-086045 made by GENCI (Grand Equipement National de Calcul Intensif) and is partially funded by the French National Research Agency (ANR) (project reference: ANR-14-CE07-0013).

References

1 A. Zakery and S. R. Elliott, *Journal of Non-Crystalline Solids*, 2003, **330**, 1–12.
2 A. B. Seddon, *Journal of Non-Crystalline Solids*, 1995, **184**, 44–50.
3 X. Zhang, B. Bureau, P. Lucas, C. Boussard-Plédel and J. Lucas, *Chemistry European Journal*, 2008, **14**, 432–442.
4 B. Bureau, C. Boussard-Plédel, P. Lucas, X. Zhang and J. Lucas, *Molecules*, 2009, **14**, 4337.
5 B. Bureau, S. Danto, H. L. Ma, C. Boussard-Plédel, X. H. Zhang and J. Lucas, *Solid State Sciences*, 2008, **10**, 427 – 433.
6 S. Danto, P. Houizot, C. Boussard-Pledel, X.-H. Zhang, F. Smektala and J. Lucas, *Advanced Functional Materials*, 2006, **16**, 1847.
7 A. A. Wilhelm, C. Boussard-Plédel, Q. Coulombier, J. Lucas, B. Bureau and P. Lucas, *Advanced Materials*, 2007, **19**, 3796.
8 Z. Yang, A. a. Wilhelm and P. Lucas, *Journal of the American Ceramic Society*, 2010, **1944**, 1941–1944.
9 P. Lucas, Z. Yang, M. K. Fah, T. Luo, S. Jiang, C. Boussard-Pledel, M.-L. Anne and B. Bureau, *Opt. Mater. Express*, 2013, **3**, 1049–1058.
10 C. Conseil, J.-C. Bastien, C. Boussard-Plédel, X.-H. Zhang, P. Lucas, S. Dai, J. Lucas and B. Bureau, *Opt. Mater. Express*, 2012, **2**, 1470–1477.
11 S. Cui, C. Boussard-Plédel, J. Lucas and B. Bureau, *Opt. Express*, 2014, **22**, 21253–21262.
12 S. R. Ovshinsky, *Phys. Rev. Lett.*, 1968, **21**, 1450–1453.
13 J. Feinleib, J. deNeufville, S. C. Moss and S. R. Ovshinsky, *Applied Physics Letters*, 1971, **18**, 254–257.
14 G.-F. Zhou, *Materials Science and Engineering: A*, 2001, **304-306**, 73 – 80.
15 N. Yamada, E. Ohno, K. Nishiuchi, N. Akahira and M. Takao, *Journal of Applied Physics*, 1991, **69**, 2849–2856.
16 S. Maurugeon, B. Bureau, C. Boussard-Plédel, A. J. Faber,

X. H. Zhang, W. Geliesen and J. Lucas, *Journal of Non-Crystalline Solids*, 2009, **355**, 2074.
17 S. Maurugeon, C. Boussard-Plédel, J. Troles, A. J. Faber, P. Lucas, X. H. Zhang, J. Lucas and B. Bureau, *J. Lightwave Technol.*, 2010, **28**, 3358–3363.
18 S. Maurugeon, B. Bureau, C. Boussard-Plédel, A. Faber, P. Lucas, X. Zhang and J. Lucas, *Optical Materials*, 2011, **33**, 660 – 663.
19 P. Jóvári, I. Kaban, B. Bureau, A. Wilhelm, P. Lucas, B. Beuneu and D. a. Zajac, *Journal of Physics: Condensed Matter*, 2010, **22**, 404207.
20 L. Rátkai, C. Conseil, V. Nazabal, B. Bureau, I. Kaban, J. Bednarcik, B. Beuneu and P. Jóvári, *Journal of Alloys and Compounds*, 2011, **509**, 5190–5194.
21 A. H. Moharram and A. M. Abdel-Baset, *Journal of Alloys and Compounds*, 2010, **508**, 37–41.
22 T. G. Edwards, E. L. Gjersing, S. Sen, S. C. Currie and B. G. Aitken, *Journal of Non-Crystalline Solids*, 2011, **357**, 3036–3041.
23 S. Sen and Z. Gan, *Journal of Non-Crystalline Solids*, 2010, **356**, 1519–1521.
24 K. Sykina, B. Bureau, L. Le Pollès, C. Roiland, M. Deschamps, C. J. Pickard and E. Furet, *Physical Chemistry Chemical Physics*, 2014, **16**, 17975.
25 S. Sen, D. C. Kaseman, I. Hung and Z. Gan, *The Journal of Physical Chemistry B*, 2015, **119**, 5747–5753.
26 C. J. Pickard and F. Mauri, *Phys. Rev. B*, 2001, **63**, 245101.
27 R. Car and M. Parrinello, *Physical Review Letters*, 1985, **55**, 2471–2474.
28 D. Marx and J. Hutter, in *Ab-initio Molecular Dynamics: Theory and Implementation*, ed. J. Grotendorst, Forschungszentrum Julich, I edn, 2000, ch. 13, pp. 301–449.
29 W. Andreoni and A. Curioni, *Parallel Computing*, 2000, **26**, 819–842.
30 D. Marx and J. Hutter, *Ab Initio Molecular Dynamics*, Cambridge University Press, 2009.
31 J. P. Perdew, K. Burke and M. Ernzerhof, *Phys. Rev. Lett.*, 1996, **77**, 3865–3868.
32 N. Troullier and J. L. Martins, *Phys. Rev. B*, 1991, **43**, 8861–8869.
33 N. Troullier and J. L. Martins, *Phys. Rev. B*, 1991, **43**, 1993–2006.
34 S. Nosé, *Molecular Physics*, 1984, **52**, 255–268.
35 W. G. Hoover, *Phys. Rev. A*, 1985, **31**, 1695–1697.
36 S. Clark, M. Segall, C. Pickard, P. Hasnip, M. Probert, K. Refson and M. Payne, *Zeitschrift fur Kristallographie*, 2005, **220**, 567–570.
37 U. Haeberlen, *High Resolution Nmr in Solids Selective Averaging*, Academic Press, New-York, 1976.
38 M. Bak, J. T. Rasmussen and N. C. Nielsen, *Journal of Magnetic Resonance*, 2011, **213**, 366 – 400.
39 B. Bureau, C. Boussard-Plédel, M. LeFloch, J. Troles, F. Smektala and J. Lucas, *Journal of Physical Chemistry B*, 2005, **109**, 6130.
40 J. Akola and R. O. Jones, *Physical Review Letters*, 2008, **100**, 205502.
41 M. Micoulaut, K. Gunasekera, S. Ravindren and P. Boolchand, *Physical Review B*, 2014, **90**, 1–9.
42 J. Y. Raty, W. Zhang, J. Luckas, C. Chen, R. Mazzarello, C. Bichara and M. Wuttig, *Nat Commun*, 2015, **6**, 7467.
43 Y.-R. Luo, *Comprehensive handbook of chemical bond energies*, FL: CRC Press, Boca Raton, 2007.
44 V. L. Deringer, W. Zhang, M. Lumeij, S. Maintz, M. Wuttig, R. Mazzarello and R. Dronskowski, *Angewandte Chemie International Edition*, 2014, **53**, 10817–10820.
45 C. Massobrio, M. Celino, P. Salmon, R. Martin, M. Micoulaut and A. Pasquarello, *Physical Review B*, 2009, **79**, 174201.
46 K. Sykina, E. Furet, B. Bureau and C. Massobrio, *Chem. Phys. Lett.*, 2012, **547**, 30–34.
47 K. Sykina, G. Yang, C. Roiland, L. Le Pollès, E. Le Fur, C. J. Pickard, B. Bureau and E. Furet, *Physical chemistry chemical physics : PCCP*, 2013, **15**, 6284–92.